Journal of Magnetism and Magnetic Materials 364 (2014) 72–79

Contents lists available at ScienceDirect

Journal of Magnetism and Magnetic Materials

journal homepage: www.elsevier.com/locate/jmmm

# Monodisperse sodium oleate coated magnetite high susceptibility nanoparticles for hyperthermia applications

R.P. Araújo-Neto [a], E.L. Silva-Freitas [a], J.F. Carvalho [a], T.R.F. Pontes [a], K.L. Silva [a], I.H.M. Damasceno [a], E.S.T. Egito [a], Ana L. Dantas [b], Marco A. Morales [c], Artur S. Carriço [c,*]

[a] Departamento de Farmácia, Universidade Federal do Rio Grande do Norte, Rua Gal. Gustavo Cordeiro de Farias s/n, Petrópolis, 59012-570 Natal-RN, Brazil
[b] Departamento de Física, Universidade do Estado do Rio Grande do Norte, 59610-210 Mossoró-RN, Brazil
[c] Departamento de Física Teórica e Experimental, Universidade Federal do Rio Grande do Norte, Campus universitrio, CEP: 59078-970 Natal-RN, Brazil

ARTICLE INFO

*Article history:*
Received 3 February 2014
Received in revised form
23 March 2014
Available online 13 April 2014

*Keywords:*
Nanoparticle
Superparamagnetic
Magnetite
Sodium oleate
Hyperthermia

ABSTRACT

We report a simple and low cost methodology to synthesize sodium oleate coated magnetite nanoparticles for hyperthermia applications. The system consists of oleate coated magnetite nanoparticles with large susceptibility (1065 emu/gT), induced by the dipolar inter-particle interaction, with a magnetic core diameter in the 6 nm–12 nm size range. In aqueous medium, the nanoparticles agglomerate to form a monodisperse system, exhibiting a mean hydrodynamic diameter of 60.6 nm ± 4.1 nm, with a low average polydispersity index of 0.128 ± 0.003, as required for intravenous applications. The system exhibits promising efficiency for magnetic hyperthermia, with a specific absorption rate of 14 W/g at a low field amplitude of 15.9 kA/m and frequency of 62 kHz. In a 50 mg/mL density in 1 mL, the temperature rises to 42.5 °C in 1.9 min.



## 1. Introduction

Cancer is one of the most challenging problems of modern medicine and a leading cause of death worldwide, accounted for 7.6 million deaths (around 13% of all-cause mortality) in 2008. Projections estimate 13.1 million deaths from cancer in 2030 [1].

Alternative techniques for cancer treatment have been widely studied in the last years to increase the effectiveness of currently available therapies, such as chemotherapy or radiotherapy, and reduce their side effects [2,3].

Hyperthermia is a promising approach for cancer therapy. Different techniques have been proposed to generate heat at the tumor site and produce apoptosis of tumor cells that are more sensitive to high temperatures than healthy cells [2,4].

The most common treatments with hyperthermia require temperature elevations to a range between 42 and 45 °C which is sufficient to destroy cancer cells without causing damage to normal tissue [5].

Much effort has been made to improve hyperthermia techniques for clinical applications, leading to the development of magnetic hyperthermia. This technique involves the administration of magnetic particles into the tumor or target tissue followed by exposure to an external AC magnetic field that causes the particles to heat because of their capacity to convert the energy absorbed from a high-frequency magnetic field into thermal energy mostly via relaxation and hysteresis losses [5–7].

Whereas the majority of hyperthermia modalities including microwave, laser and ultrasonic wave-based treatments are restricted in their utility because of unwanted heating of healthy tissue, magnetic hyperthermia has the advantage to selectively target the tumor cells [4,8].

The frequency of the AC magnetic field has to be higher than 50 kHz, to avoid neuromuscular electrostimulation, and lower than 10 MHz for appropriate penetration into the body [6]. High amplitude and frequency of the applied field may generate eddy currents and cause non-selective heating of the biological tissue, so a limit on the amplitude of magnetic field was established between 8 and 16 kA/m [2].

In addition to the potential use in hyperthermia, magnetic particles have attracted much attention due to their current and novel biomedical applications such as magnetic resonance imaging, tissue engineering, magnetofection, and cellular labeling/cell separation and magnetically targeted drug delivery [9–13].

For clinical applications, these particles must be biocompatible, non-toxic, non-immunogenic and water-based [14]. Several studies report a vast range of magnetic materials that can be applied in biotechnology. Iron oxide particles represented by magnetite ($Fe_3O_4$) and maghemite ($\gamma$-$Fe_2O_3$) are considered promising candidates because they present biocompatibility, high saturation magnetization, stable magnetic response, higher resistance to

* Corresponding author.
*E-mail addresses:* ascarrico@gmail.com, acarrico@dfte.ufrn.br (A.S. Carriço).

http://dx.doi.org/10.1016/j.jmmm.2014.04.001
0304-8853/

oxidation than other metal compounds and relative easiness to functionalize with polymers or functional groups [15,16].

The size also plays a key role. Nanoparticles with small diameter and narrow size distribution are required for biomedical applications in general. It is currently accepted that the diameter of the nanoparticles should be in the 10–100 nm size range, in order to avoid rapid removal from systemic circulation by extravasation, renal clearance or uptake into the reticuloendothelial system, and emboli within the capillaries [17,18].

For magnetic hyperthermia applications, the need to control the particle size is further enhanced, in order to optimize the energy transfer to the biologic tissue. High polydispersity of the nanoparticles size diminishes the magnetic heating that can be achieved [19,20].

Due to the high surface area to volume ratio, and the strong dipole–dipole interactions and van der Waals attractive forces, magnetic nanoparticles tend to agglomerate and form large clusters resulting in increased particle size [21].

Surface coating of the nanoparticles prevents aggregation and may provide colloidal stability by steric and/or electrostatic repulsion [22].

Numerous coating materials have been reported previously, such as polymers (e.g., polyethylene glycol, Pluronic®, dextran, chitosan), inorganic materials (e.g., silica, alumina), and liposome and fatty acids [22–24].

Previous works report that oleic acid and sodium oleate have high affinity to the surface of iron oxide particles, being effective in the stabilization of nanoparticles by steric repulsion. It is possible to obtain iron oxide nanoparticles coated with monolayers of these surfactants, which are dispersible in organic solvents, or bilayers that can be dispersed in water. In the latter case, the primary layer is first adsorbed onto the surface of the nanoparticles through chemical bonds between the carboxylic acid head groups of the surfactant molecules and the particle surface. The secondary layer is adsorbed onto the primary layer through hydrophobic interactions. Thus, the outermost layer provides hydrophilic groups that make the magnetic nanoparticles dispersible in aqueous solutions [25–29].

We note that toxicity evaluation is a mandatory issue. Sun et al. [30] reported that magnetite nanoparticles coated with sodium oleate had low toxicity and a better biocompatibility than magnetite nanoparticles coated with polyethylene glycol. Jain et al. evaluated the distribution, clearance and biocompatibility of iron oxide magnetic nanoparticles coated with oleic acid and Pluronic® in rats [31]. They found that the coated nanoparticles did not cause long-term changes in the liver enzyme levels, or induce oxidative stress, and thus can be safely used for drug delivery and imaging applications without significant levels of toxicity.

We presently report the synthesis of superparamagnetic sodium oleate coated magnetite nanoparticles, using a simple and low cost co-precipitation methodology, with no organic solvents. In the aqueous medium the nanoparticle system has a narrow size distribution, and large initial susceptibility, as required for high efficiency hyperthermia applications.

## 2. Materials and methods

Iron (III) chloride hexahydrate ($FeCl_3 \cdot 6H_2O$, 99%), iron (II) sulphate heptahydrate ($FeSO_4 \cdot 7H_2O$, 99%), ammonium hydroxide (28–30% $NH_3$), potassium bromide (KBr, 99%) and ethanol ($C_2H_6O$, 99%) were purchased from Vetec (Vetec Química Fina Ltda., Brazil). Sodium oleate ($C_{18}H_{33}NaO_2$, 82%) was acquired from Sigma (Sigma-Aldrich Co. LLC., USA). Deionized water was prepared using a DE-1800 water purification system (Permution Ltda., Brazil).

The nanoparticles were synthesized by co-precipitation of $Fe^{3+}$ and $Fe^{2+}$ salts using excess of ammonium hydroxide as previously described [26,32]. In a typical synthesis, an aqueous solution containing 0.12M of $Fe^{3+}$ and 0.06M of $Fe^{2+}$ was prepared by dissolution of $FeCl_3 \cdot 6H_2O$ and $FeSO_4 \cdot 7H_2O$ in deionized water.

This solution was heated until 80 °C and stirred at 960 rpm (Mechanical stirrer RW 20, IKA Labortechnik, Germany), followed by rapid addition of 16 mL of $NH_4OH$ (28–30% $NH_3$) solution. The resulting suspension was vigorously stirred for 5 min. Then, 50 mL of 0.06 M sodium oleate dispersion was added into the reaction medium and continuously stirred for 25 min. At the end of the process, a black precipitate was obtained and washed several times with deionized water.

Finally, the procedure was repeated one more time by heating the precipitate in aqueous suspension until 80 °C with stirring at 960 rpm and subsequent addition of 50 mL of a sodium oleate dispersion with the same concentration as the previous one. At this point, it was observed the formation of a stable dispersion that was stirred for 25 min.

Additionally, bare magnetic particles were prepared by the same process described above without the step of coating with sodium oleate, in order to analyze its influence in the stabilization of magnetic nanoparticles. While the sodium oleate coated particles showed colloidal aspect with good dispersion in water and no evident sedimentation, the uncoated particles easily precipitated to the bottom of the flask.

## 3. Characterization

A particle size analyzer (ZetaPALS, Brookhaven Instruments) was used to measure size distribution of the particles by dynamic light scattering (DLS) technique. The zeta potential (ZP) was determined in the same equipment.

X-ray diffraction (XRD) analysis (MiniFlex™II, Rigaku Co.) using CuK$\alpha$ radiation ($\lambda = 1.54060$ Å) and $2\theta$ scan range from 15–80° was employed to study the crystal structure of the samples.

A vibrating sample magnetometer (VSM, custom-made) was used to measure the magnetization of the samples at room temperature with fields up to 1.2 T.

The structure, morphology and size of the crystallites were investigated by selected area of electron diffraction (SAED) and transmission electron microscopy (TEM) with an acceleration voltage of 120 kV (Tecnai™ $G^2$ Spirit TWIN, FEI). The samples were prepared by placing one drop of the dispersion on a carbon coated copper grid (300 mesh) and the size distribution was calculated from 20 different TEM images using an image analysis software (ImageJ) by measuring the diameters of a total of 500 particles.

To study the interactions between surfactant and surface of the particles, the Fourier transform infrared (FTIR) spectra were recorded in transmittance mode over the wavenumber range of 400–4000 $cm^{-1}$ at a resolution of 1 $cm^{-1}$ (Spectrum 65 FTIR Spectrometer, PerkinElmer Inc.). The powdered samples were mixed with KBr and compressed into a pellet. For this particular analysis, extra samples were produced by submitting the sodium oleate coated particles to several washings with ethanol to remove any surfactant molecule that was not chemically bound to the surface of the particles.

The surfactant mass of coated particles was quantified by thermogravimetric analysis (TGA) under argon atmosphere (50 mL/min argon flow) from room temperature up to 500 °C with a heating rate of 10 °C/min (DTG-60H, Shimadzu). Differential thermal analysis (DTA) was employed using the same parameters.

The evaluation of the particles potential application in magnetic hyperthermia was performed in an experimental setup which produces an alternating magnetic field with a frequency of 62 kHz and amplitude of 15.9 kA/m or 200 Oe. The samples were subjected to this field for 600 s and their temperature was

measured every second. In this test, the ferrofluid had a particle concentration of approximately 50 mg/mL in 1 mL volume.

## 4. Results and discussion

### 4.1. Dynamic light scattering

The size distribution of the particles coated with sodium oleate as measured by DLS is shown in Fig. 1a. The mean hydrodynamic diameter of the nanoparticles was 60.6 nm ± 4.1 nm. It was also calculated that 10%, 50% and 90% of the nanoparticles were smaller than 31.1 nm ± 1.7 nm, 46.9 nm ± 2.9 nm and 70.7 nm ± 4.7 nm, respectively.

The polydispersity index (PDI) was determined with an average value of 0.128 ± 0.003. PDI less than 0.2 indicates a monodisperse particulate system, as required for intravenous applications [33].

For the uncoated magnetic particles (Fig. 1b), the mean hydrodynamic diameter was 1230.4 nm ± 165.7 nm, and 10%, 50% and 90% of the particles were smaller than 804.6 nm ± 367.3 nm, 1224.8 nm ± 160.4 nm and 2020 nm ± 505.3 nm, respectively. The average value of PDI was 0.418 ± 0.008 which characterizes a polydisperse particulate system.

These results confirm the essential role of sodium oleate coating of the magnetite particles, leading to a monodisperse nanoparticle system. The absence of surfactant led to an increase of about 20 times in the average particle hydrodynamic diameter, combined with a considerable increment in polydispersity of more than three times. Furthermore, for the same experimental conditions, the uncoated particles exhibited a relative size variation much larger than the coated nanoparticles, as observed in the standard deviation values, indicating that the particle aggregation can take place differently for each synthesis process when no surfactant is used.

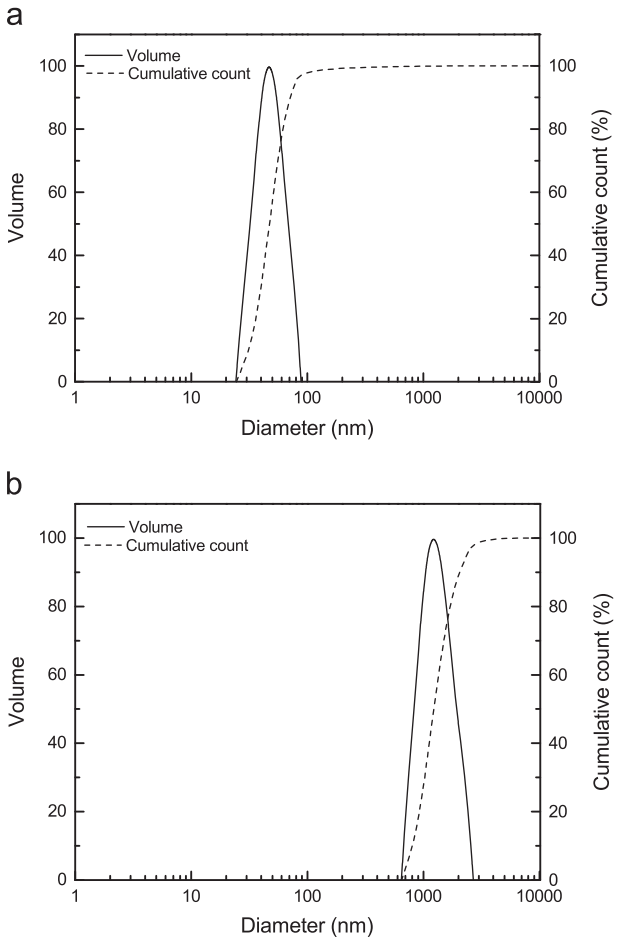


**Fig. 1.** Hydrodynamic size distribution of (a) coated nanoparticles and (b) uncoated microparticles.

### 4.2. Zeta potential

Zeta potential measurements for coated nanoparticles revealed an average value of −32.9 ± 1.6 mV, while for the bare microparticles this value was +5.2 ± 0.4 mV. The negative zeta potential of the coated nanoparticles can be attributed to the negatively charged carboxylate groups present in the sodium oleate. As the pKa of carboxyl group is about 4, in aqueous medium with pH higher than 6 virtually all carboxyl groups are ionized to the form of carboxylate [34].

Zeta potential values found below −30 mV indicate that in addition to stabilization by steric repulsion, the sodium oleate can also stabilize the particles by electrostatic repulsion mechanisms. Concerning the uncoated micropaticles, the positive and relatively low zeta potential is related to the fact that the point of zero charge (PZC) admitted for iron oxide particles is approximately 7.9. Therefore, pH values below PZC lead to a positive zeta potential which increases as the pH reduces [27].

### 4.3. X-ray diffraction

XRD patterns of the coated nanoparticles and standard magnetite (JCPDS Card no. 19-0629) are shown in Fig. 2a and b. The analysis of the position and relative intensity of diffraction peaks suggests the formation of magnetite nanoparticles. However, due to the similarity between $Fe_3O_4$ and γ-$Fe_2O_3$ inverse spinel crystal structure, this analysis may not distinguish which of the iron oxides was actually formed [35]. One might think of using the position of 440 peak in order to identify the predominant magnetic phase. The 440 peak position is around 62.5° for magnetite (JCPDS Card no. 19-0629) and 62.9° for maghemite (JCPDS Card no. 39-1346). In our samples the 440 peak position was 62.7° indicating either the presence of both magnetic phases, or the formation of non-stoichiometric magnetite nanoparticles with crystal defects.

For this reason we calculated the lattice parameter of the crystals. The typical unit cell parameter reported for maghemite is 8.34 Å and for magnetite is 8.39 Å [36]. The XRD data revealed nanoparticles with lattice parameter of 8.383 Å that indicates the synthesis of magnetite particles.

The lower value of lattice parameter observed in the nanoparticles prepared by co-precipitation could be explained by oxidation

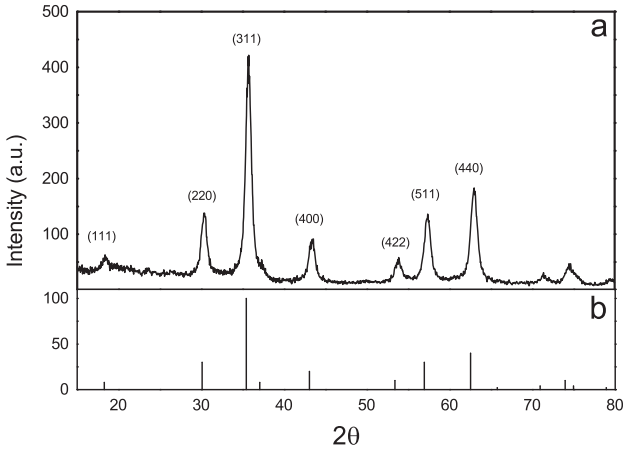


**Fig. 2.** XRD patterns of (a) coated nanoparticles and (b) pure magnetite.

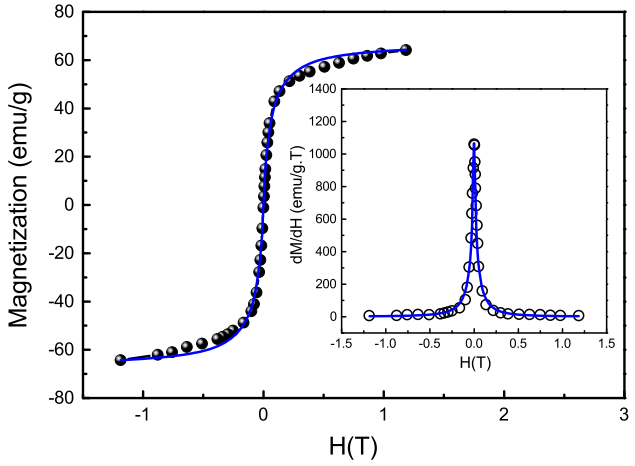


**Fig. 3.** Magnetization curve of magnetite nanoparticles, full and open symbol curves for the experimental results and continuum line for the theoretical model. In the inset we show the susceptibility.

of $Fe^{2+}$ or existence of small amount of maghemite impurities, especially at the surface of the particles [36,37].

The mean crystallite size, calculated from the XRD pattern, is 9.8 nm. This value is within the 25 nm size limit required for superparamagnetism of magnetite at room temperature [38].

The DLS and XRD data indicate that in the aqueous phase the crystallites agglomerate forming a monodisperse ferrofluid with larger particles of 60 nm size.

### 4.4. Magnetization

The magnetization, as shown in Fig. 3, exhibits a value of about 64 emu/g at an external field strength of 1.2 T. This is about 69% of the bulk saturation magnetization of magnetite (92 emu/g). Furthermore, the magnetization does not saturate for this large value of the external field strength. Both results are signatures of small size superparamagnetic nanoparticle systems [28,35,39].

The reduced value of magnetization may be partially attributed to dilution effects, caused by the presence of the sodium oleate adsorbed layer.

Furthermore, the magnetic moment of small size nanoparticles may have a relevant reduction due to the existence of spin canting in the near surface region. This effect is more pronounced in small particles, which have a much larger fraction of surface spins. A disordered alignment of surface atomic spins may be induced by the reduced surface coordination and the broken exchange bonds in the near surface layers [40].

As shown in Fig. 3 remanence and coercivity are nearly zero, indicating a typical superparamagnetic behavior. For biomedical applications, superparamagnetic particles are preferred because they do not retain any magnetization after removal of the magnetic field [4].

In order to model the magnetization curve we use a self-consistent method which takes into account the existence of nanoparticles with dimensions in the 5 nm to 18 nm size range, with a size dispersion close to that found in the analysis of the TEM images. The model also accounts for the dipolar interaction of the nanoparticles assembled together in the VSM sample holder.

The basic phenomenology is based on the fact that in the presence of an external magnetic field each superparamagnetic particle produces its own dipolar field. Therefore each one of the particles is under the action of the applied field and the effective dipolar field produced by all the other particles.

The effective dipolar field, for a given value of the applied field, depends on the relative position of the particles in the VSM sample holder, the VSM sample holder shape, as well as on the size dispersion.

Furthermore, the effective dipolar field acting on a given nanoparticle also depends on the diameters of the particles distributed in the first, second, third shells of particles around it. We adopted a simplifying assumption.

The thermal average value of the magnetization is represented by an average over a distribution of superparamagnetic spherical crystallites, each of which is considered to be subjected to the thermal average dipolar field of the others.

For a given value of the external field, the magnetization is given by

$$M(H) = M_S \int \mathcal{L}\{\mu(D)\mathcal{H}_{eff}/k_BT\} f(D)\, dD \tag{1}$$

where $\mathcal{L}$ is the Langevin function, $M_S$ is the saturation magnetization, $\mu(D) = \pi M_S D^3/6$ is the saturation magnetic moment of a nanoparticle of diameter $D$, and $f$ is a log-normal distribution function.

$\mathcal{H}_{eff}$ includes the external field $H$, and an effective dipolar field, $\mathcal{H}_{eff} = H + \mathcal{H}_d$. We assumed that the effective dipolar field $\mathcal{H}_d$ is proportional to the thermal average dipolar field produced by the crystallite at a distance of one diameter, $\mathcal{H}_d = 2\alpha\langle\mu(D)\rangle/D^3$. $\langle\mu(D)\rangle$ is the thermal average magnetic moment of the crystallites with diameter $D$.

We have assumed a reduction of the nanoparticles saturation magnetic moment down to 70% of the saturation value. M(H), $\alpha$ and the distribution function were adjusted self-consistently to fit the experimental data. We have found a narrow log-normal distribution function

$$f(d) = \frac{1}{\sqrt{2\pi}\sigma D} \exp\left[\frac{-\ln (D/D_0)^2}{2\sigma^2}\right] \tag{2}$$

with a standard deviation $\sigma = 0.24$ and a $D_0 = 8.0$ nm median diameter, with 83% of the particles with diameter in the 6 nm–12 nm range, and an average diameter of 8.3 nm, in agreement with the X-ray results and the TEM images size analysis.

In Fig. 3 we show the magnetization curve and susceptibility of the coated magnetite nanoparticles. Notice that the theoretical model (continuum line curves) reproduces quite well the experimental results. Both the magnetization curve and the initial susceptibility are well represented in the model theory.

We have found that the dipolar interaction between the crystallites plays a key role in the magnetic response of the nanoparticles to external field in the mT range, and leads to the large value of the initial susceptibility (1065 emu/gT). Without the dipolar interaction, we have found that the initial susceptibility is smaller than the measured value.

A discussion of the low field effects is appropriate since biomedical safety requires an AC magnetic field strength of at most 20 mT [2]. Also, the specific absorption rate for superparamagnetic particles is proportional to the value of the magnetic susceptibility at small field strength [7].

Before entering the detailed discussion of this point, it is instructive to consider qualitatively the phenomenology which leads to the response of the nanoparticle system to a small strength external field. This is a key issue for hyperthermia applications.

Magnetite has a magnetic moment of $16.4\mu_B$ per unit cell of 0.295 $nm^3$ volume [41]. Thus a magnetite nanoparticle with diameter $D$ has a saturation magnetic moment given by $\mu_0 = 55.59\pi D^3/6$.

In the presence of a magnetic field $H$, an isolated superparamagnetic particle has a thermal average magnetic moment, along the field direction, which may be estimated [41] as

$$\mu = \mu_0 \mathcal{L}\{\mu_0 H/k_BT\} \tag{3}$$

where $\mu_0$ is the saturation moment, and $\mathcal{L}$ is the Langevin function, $\mathcal{L}(x) = \coth(x) - 1/x$.

A 9 nm diameter magnetite particle has a saturation magnetic moment of around $7.07 \times 10^4 \mu_B$. At room temperature, an external field of 1 mT strength is enough to break the thermal relaxation balance, producing a thermal average net magnetic moment of around 1.0% of the saturation value. This amounts to stabilizing $92\mu_B$ per 9 nm diameter particle. At a distance of 9 nm from the particle center, the dipolar field is about 8 mT. For small external field strengths, the dipolar field produced by the 9 nm magnetite nanoparticle at its neighborhood is of the order of magnitude of the external field.

Thus, in the low field range, the dipolar effects cannot be neglected. In the mT field range, the susceptibility is to a large extent controlled by the dipolar interaction between the crystallites.

In order to investigate the impact of the dipolar interaction on the magnetization, we have compared the final result shown in Fig. 3 with simulations using the same algorithm, but with different size distribution functions and effective dipolar interaction fields.

Using the same size distribution function (Eq. (2), with $\sigma = 0.24$ and $D_0 = 8.0$ nm), but no dipolar contribution to the effective ($\mathcal{H}_{eff} = H$), we have reproduced most of the magnetization curve, except in the low field range. The initial susceptibility was found to be only 61% of the measured value.

We have also checked monodisperse nanoparticle systems with size in the 6 nm–12 nm range. Without dipolar interaction, a 9 nm particle system ($\sigma = 0.01$ and a $D_0 = 9.0$ nm) has an initial susceptibility of 713 emu/gT, which is about 66% of the measured value.

In order to reproduce the large initial susceptibility value, a large diameter monodisperse particle system ($\sigma = 0.01$ and a $D_0 = 10.3$ nm) is required. However, this is not appropriate. In this case the magnetization saturates too early, at an external field value of about 500 mT.

A previous report has indicated that for nanoparticle systems with similar diameter size distribution, the dipolar interaction leads not only to larger initial susceptibility, but also to a small coercivity of 22 mT [42].

The dipolar effects in our coated samples are smaller due to the oleate bilayer, which leads to a relevant decrease in the average particle density. However, it is large enough to increase the susceptibility by a factor of almost two.

### 4.5. Transmission electron spectroscopy

Fig. 4 shows two transmission electron microscopy (TEM) pictures, selected from a total of 20 images used to investigate the size distribution of the oleate coated magnetite nanoparticles.

The size histogram, including a total of 500 nanoparticles, shows magnetite nanoparticles with dimensions in the 5 nm–18 nm size range, and corresponds to a log-normal distribution with median diameter of 9.8 nm, standard deviation $\sigma = 0.244$, and an average diameter of 10.01 nm.

This narrow size distribution, with about 80% of the nanoparticles in the 6 nm–12 nm range of diameters, is in good agreement with the crystallite size (9.8 nm) estimated from the X-ray diffractogram.

From the SAED pattern of the synthesized sample shown in Fig. 5, the d-spacings corresponding to the respective Miller indices (hkl) were determined as being 4.86 Å (111), 2.97 Å (220), 2.52 Å (311), 2.08 Å (400), 1.69 Å (422), 1.61 Å (511) and 1.47 Å (440). These values were close to those found in standard magnetite (JCPDS Card no. 19-0629) which are 4.85 Å (111), 2.97 Å (220), 2.53 Å (311), 2.10 Å (400), 1.71 Å (422), 1.62 Å (511) and 1.48 Å (440). The diffraction pattern is in agreement with the XRD data.

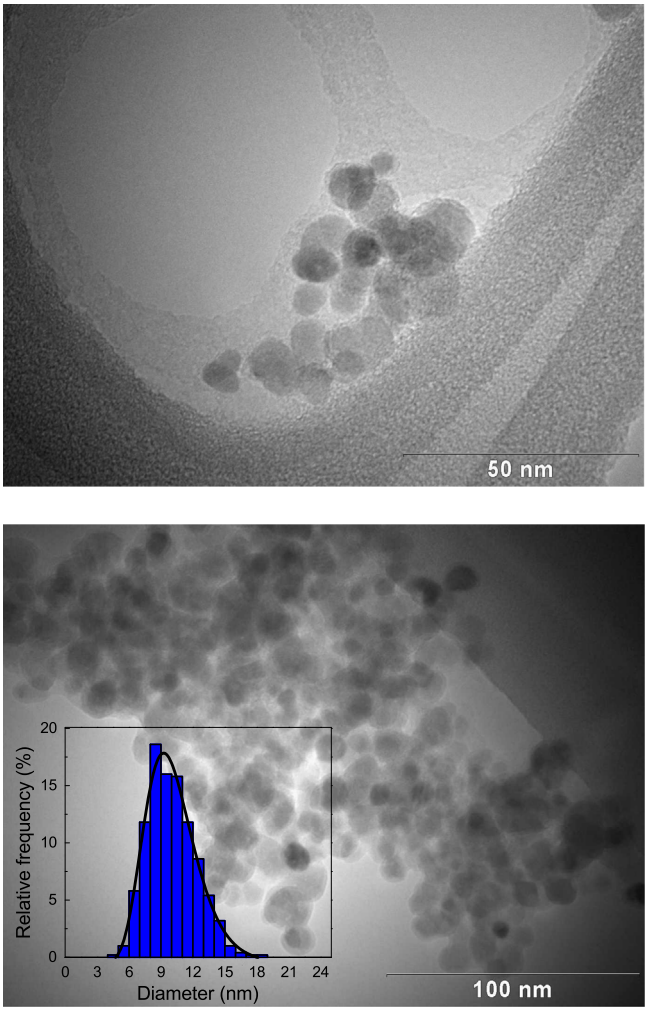


**Fig. 4.** TEM image and size distribution histogram of oleate coated nanoparticles.

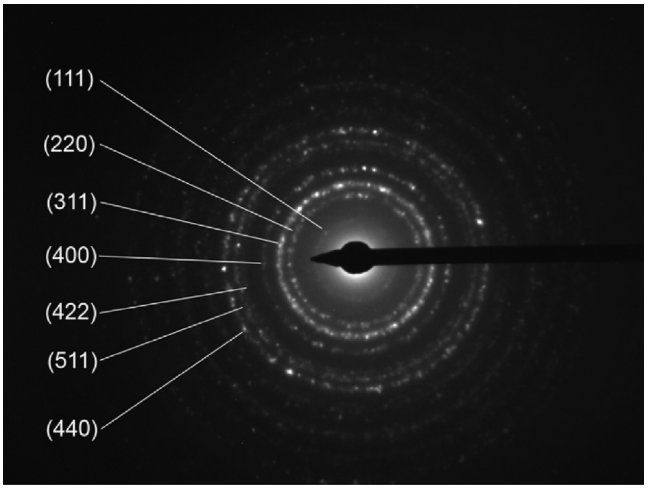


**Fig. 5.** Selected area electron diffraction (SAED) pattern of oleate coated nanoparticles.

### 4.6. Fourier transform infrared spectroscopy

FTIR spectra of the prepared samples are presented in Fig. 6. Spectral bands with a maximum transmittance at 437 $cm^{-1}$ and 580 $cm^{-1}$ correspond, respectively, to the vibration of the $Fe^{3+}$–O and $Fe^{2+}$–O bonds in the crystalline lattice of $Fe_3O_4$ [43].

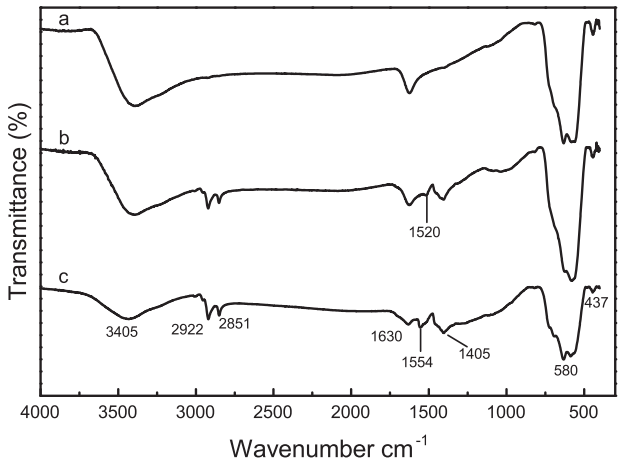


**Fig. 6.** FTIR spectra of (a) magnetite particles without coating, (b) coated nanoparticles washed with ethanol to remove physically adsorbed sodium oleate and (c) coated nanoparticles.

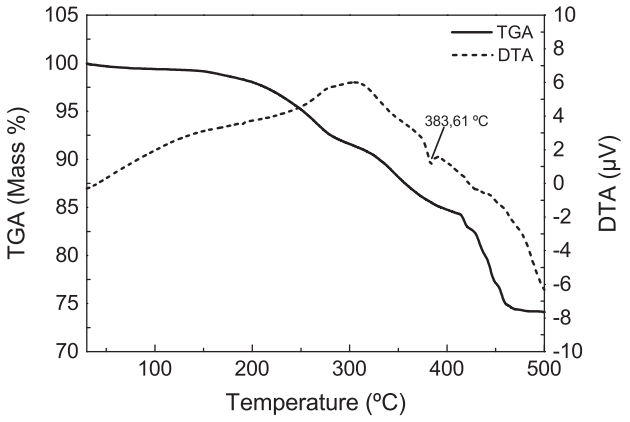


**Fig. 7.** TGA and DTA curves of coated nanoparticles.

The bands at 1405 $cm^{-1}$ and 1554 $cm^{-1}$ can be ascribed to the symmetric $\nu_s(COO^-)$ and asymmetric $\nu_{as}(COO^-)$ carboxylate stretches. The sharp bands at 2922 $cm^{-1}$ and 2851 $cm^{-1}$ are attributed to asymmetric and symmetric C–H vibrations of the methylene groups.

During the preparation of $Fe_3O_4$ nanoparticles by the chemical co-precipitation, their surfaces may be covered with hydroxyl groups in an aqueous environment. Thus, the characteristic bands of hydroxyl groups, 1630 $cm^{-1}$ and 3405 $cm^{-1}$, appeared in the FTIR spectra [26,44,45].

The spectrum in Fig. 6b shows the presence of bands corresponding to $CH_2$ and $COO^-$ groups, suggesting that the sodium oleate is actually chemically bound to the surface of the magnetic nanoparticles.

On the other hand, the band assigned to the asymmetric vibration of carboxylate group shifted down to 1520 $cm^{-1}$ and had an intensity reduction, indicating that there were oleate molecules freely dispersed in the aqueous medium, or free terminal carboxylate groups forming a surfactant bilayer. This hypothesis is supported by the good dispersion of the nanoparticles in water.

The type of interaction between the carboxylate group and the nanoparticle surface can be determined by the wavenumber separation, $\Delta\nu$, between the symmetric $\nu_s(COO^-)$ and asymmetric $\nu_{as}(COO^-)$ FTIR bands. The $\Delta\nu$ (1520–1405 = 115 $cm^{-1}$) found was ascribed to chelating bidentate coordination in which the interaction between the $COO^-$ group and the Fe atom was covalent [28,44].

### 4.7. Thermogravimetric and differential thermal analysis

TGA provided additional quantitative evidence of the magnetic nanoparticles coating. The initial weight loss of 1.5% is due to the evaporation of physically adsorbed water or degradation of surface hydroxyl groups (Fig. 7). Subsequent weight loss of 24.63% corresponds to decomposition of the surfactant [46]. We note that previous studies showed that the number of surfactant molecules adsorbed on the magnetite surface may vary from 2 to 3.5 molecules/$nm^2$ [47]. Thus, for functionalized magnetite nanoparticles with 10 nm diameter the amount corresponding to the surfactant are of the order of 25% of the total mass.

The major weight loss transitions of magnetic nanoparticles occurred between 200 and 450 °C in a two-step process that might indicate the formation of an oleate bilayer on the magnetite surface. In this case, a secondary layer physically adsorbed into a primary layer is decomposed at lower temperatures while the primary layer chemically bound to the particle surface undergoes desorption/decomposition at higher temperatures [48]. The DTA data suggest that the latter process starts at 383 °C.

### 4.8. Heat dissipation

The specific absorption rate (SAR), which is the amount of energy converted into heat, per unit time, per unit Fe mass, is given by [49]

$$SAR = c\frac{\Delta T}{\Delta t}\frac{1}{m_{Fe}} \quad (4)$$

where $c$ is the sample heat capacity, calculated as a mass weighted mean value of magnetite and water, $\Delta T/\Delta t$ is the initial slope of the time-dependent temperature curve, and $m_{Fe}$ is the iron content per gram of the ferrofluid.

The mean SAR value of the oleate coated nanoparticles was about 14 W/g at a low field amplitude of 15.9 kA/m and frequency of 62 kHz. Rashad et al. managed to obtain similar results with a lower particle concentration, although a much larger magnetic field with 41.5 kA/m amplitude and 160 kHz frequency was employed [50].

Typical SAR values between 10 and 100 W/g are commonly reported for superparamagnetic ferrofluids with low particle concentration and small crystallite sizes submitted to alternating magnetic fields up to 18 kA/m [2–4].

Fig. 8 shows the time-dependent temperature curve of the samples in the AC magnetic field, with a frequency of 62 kHz and amplitude of 15.9 kA/m. We have used a ferrofluid concentration of 50 mg/mL in a 1 mL volume of water. The sample temperature increases rapidly, reaching 42.5 °C in about 1.9 min.

We suggest that the rapid temperature increase, for low values of the amplitude and frequency of the AC field, originates in the dipolar interaction between the 9 nm crystallites that compose the 60 nm nanoparticles.

This interpretation is corroborated by previous works on the impact of the dipolar interaction on the specific absorption rate of dextran coated iron oxide nanoparticles [51–53].

There are also interesting reports on the effects of particle interactions on the cooperative behavior of multicore nanoparticles ferrofluids for hyperthermia [54,55]. Lartigue et al. have found that the magnetic ordering and exchange interactions within the multicore nanostructures may lead to a 10-fold SAR increase for multicore nanoparticle systems with respect to that of single core materials [54].

## 5. Conclusions

In summary, we have reported the synthesis and characterization of oleate coated magnetite nanoparticles with a narrow size distribution, as appropriate for magnetic hyperthermia applications.

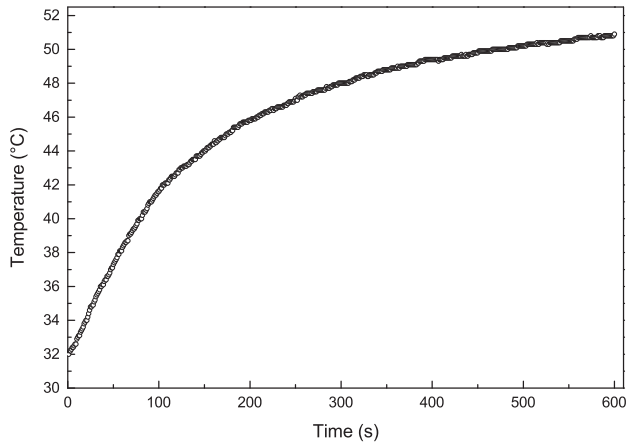


**Fig. 8.** Time-dependent temperature curve of coated nanoparticles.

The synthesis is based on a simple and inexpensive co-precipitation method with the temperature selected to optimize the oleate coverage of the magnetite nanoparticles.

We have shown that sodium oleate successfully coated the magnetite nanoparticles, in a weight ratio of about 25%, promoting their stabilization into a system with narrow size distribution, with 80% of the crystallites with dimensions in the 6 nm–12 nm range, and average size around 9 nm.

Furthermore the DLS measurements indicate a satisfactory pattern of agglomeration of the nanoparticles in aqueous medium. The mean hydrodynamic diameter of the nanoparticles is 60.6 nm $\pm$ 4.1 nm, with a small average polydispersity index (PDI) of 0.128 $\pm$ 0.003, as required for safe intravenous applications.

We have also shown that the magnetization measurements in powder samples correspond to a system of dipolar coupled magnetite crystallites, with dimensions ranging from 6 nm to 18 nm, with 83% of the particles in the 6 nm–12 nm range, in agreement with the particle size analysis from TEM images.

The agglomeration of the crystallites in the 60 nm nanoparticles is stable upon heating up to 200 °C. The basic structure is maintained even when the coated nanoparticles are dried at 100 °C to obtain a solid sample, since the TGA data suggest that the surfactant is not decomposed until 200 °C, and when the dried samples are redispersed in water, the colloidal aspect is reproduced.

The system exhibits promising efficiency for magnetic hyperthermia, with a specific absorption rate of 14 W/g at a low field amplitude of 15.9 kA/m and frequency of 62 kHz. The sample temperature increases rapidly, reaching 42.5 °C in about 1.9 min.

We argue that the rapid heating results from the strong dipolar interactions between the crystallites within the 60 nm nanoparticles, leading to a collective behavior of the crystallites.

## Acknowledgments

This research was partially supported by the Brazilian research agencies CAPES and CNPq. The work of A.S.C. was supported by CNPq Grant No. 350773. The work of A.L.D. was supported by CNPq Grant No. 309676. The authors acknowledge technical support from Dr. Geronimo Perez, Mr. Carlos Iglesias and the staff from NUPEG/UFRN and Dimat/INMETRO.

## References

[1] WHO, Cancer: GLOBOCAN, IARC (2013), Accessed: October 23, 2013, ⟨http://www.who.int/mediacentre/factsheets/fs297/en/index.html⟩.
[2] C.S.S.R. Kumar, F. Mohammad, Magnetic nanomaterials for hyperthermia-based therapy and controlled drug delivery, Adv. Drug Del. Rev. 63 (2011) 789–808.
[3] R. Hergt, S. Dutz, R. Müller, M. Zeisberger, Magnetic particle hyperthermia: nanoparticle magnetism and materials development for cancer therapy, J. Phys.: Condens. Matter 18 (2006) S2919.
[4] S. Laurent, S. Dutz, U.O. Häfeli, M. Mahmoudi, Magnetic fluid hyperthermia: focus on superparamagnetic iron oxide nanoparticles, Adv. Colloid Interface Sci. 166 (2011) 8–23.
[5] E. Pollert, P. Veverka, M. Veverka, O. Kaman, K. Záveta, S. Vasseur, R. Epherre, G. Goglio, E. Duguet, Search of new core materials for magnetic fluid hyperthermia: preliminary chemical and physical issues, Prog. Solid State Chem. 37 (2009) 1–14.
[6] S. Mornet, S. Vasseur, F. Grasset, P. Veverka, G. Goglio, A. Demourgues, J. Portier, E. Pollert, E. Duguet, Magnetic nanoparticle design for medical applications, Prog. Solid State Chem. 34 (2006) 237–247.
[7] R.E. Rosensweig, Heating magnetic fluid with alternating magnetic field, J. Magn. Magn. Mater. 252 (2002) 370–374.
[8] Q.A. Pankhurst, J. Connolly, S.K. Jones, J. Dobson, Applications of magnetic nanoparticles in biomedicine, J. Phys. D: Appl. Phys. 36 (2003) R167.
[9] C. Alexiou, R. Tietze, E. Schreiber, R. Jurgons, H. Richter, L. Trahms, H. Rahn, S. Odenbach, S. Lyer, Cancer therapy with drug loaded magnetic nanoparticles-magnetic drug targeting, J. Magn. Magn. Mater. 323 (2011) 1404–1407.
[10] M. Mahmoudi, S. Sant, B. Wang, S. Laurent, T. Sen, Superparamagnetic iron oxide nanoparticles (SPIONs): development, surface modification and applications in chemotherapy, Adv. Drug Del. Rev. 63 (2011) 24–46.
[11] A.K.A. Silva, E.L. Silva, J.F. Carvalho, T.R.F. Pontes, R.P. Araújo Neto, A. Silva Carriço, E.S.T. Egito, Drug targeting and other recent applications of magnetic carriers in therapeutics, Key Eng. Mater. 441 (2010) 357–378.
[12] E.L. Silva, J.F. Carvalho, T.R.F. Pontes, E.E. Oliveira, B.L. Francelino, A.C. Medeiros, E.S.T. Egito, J.H. Araujo, A.S. Carriço, Development of a magnetic system for the treatment of Helicobacter pylori infections, J. Magn. Magn. Mater. 321 (2009) 1566–1570.
[13] M. Yu, J. Park, S. Jon, Magnetic nanoparticles and their applications in image-guided drug delivery, Drug Deliv. Transl. Res. 2 (2012) 3–21.
[14] U.O. Häfeli, Magnetically modulated therapeutic systems, Int. J. Pharm. 277 (2004) 19–24.
[15] A.K. Gupta, M. Gupta, Synthesis and surface engineering of iron oxide nanoparticles for biomedical applications, Biomaterials 26 (2005) 3995–4021.
[16] N. Tran, T.J. Webster, Magnetic nanoparticles: biomedical applications and challenges, J. Mater. Chem. 20 (2010) 8760–8767.
[17] M.E. Davis, Z. Chen, D.M. Shin, Nanoparticle therapeutics: an emerging treatment modality for cancer, Nat. Rev. Drug Discov. 7 (2008) 771–782.
[18] T. Neuberger, B. Schof, H. Hofmann, M. Hofmann, B. von Rechenberg, Superparamagnetic nanoparticles for biomedical applications: possibilities and limitations of a new drug delivery system, J. Magn. Magn. Mater. 293 (2005) 483–496.
[19] A.P. Khandhar, R.M. Ferguson, K.M. Krishnan, Monodispersed magnetite nanoparticles optimized for magnetic fluid hyperthermia: implications in biological systems, J. Appl. Phys. 109 (2011) 7B310–317B3103.
[20] B. Luigjes, S.M.C. Woudenberg, R. de Groot, J.D. Meeldijk, H.M. Torres Galvis, K.P. de Jong, A.P. Philipse, B.H. Erné, Diverging geometric and magnetic size distributions of iron oxide nanocrystals, J. Phys. Chem. C 115 (2011) 14598–14605.
[21] C. Rümenapp, B. Gleich, A. Haase, Magnetic nanoparticles in magnetic resonance imaging and diagnostics, Pharm. Res. 29 (2012) 1165–1179.
[22] A. Tomitaka, T. Koshi, S. Hatsugai, T. Yamada, Y. Takemura, Magnetic characterization of surface-coated magnetic nanoparticles for biomedical application, J. Magn. Magn. Mater. 323 (2011) 1398–1403.
[23] Z. Karimi, L. Karimi, H. Shokrollahi, Nano-magnetic particles used in biomedicine: core and coating materials, Mater. Sci. Eng. C 33 (2013) 2465–2475.
[24] J.K. Oh, J.M. Park, Iron oxide-based superparamagnetic polymeric nanomaterials: design, preparation, and biomedical application, Prog. Polym. Sci. 36 (2011) 168–189.
[25] A. Tomitaka, K. Ueda, T. Yamada, Y. Takemura, Heat dissipation and magnetic properties of surface-coated $Fe_3O_4$ nanoparticles for biomedical applications, J. Magn. Magn. Mater. 324 (2012) 3437–3442.
[26] K. Yang, H. Peng, Y. Wen, N. Li, Re-examination of characteristic FTIR spectrum of secondary layer in bilayer oleic acid-coated $Fe_3O_4$ nanoparticles, Appl. Surf. Sci. 256 (2010) 3093–3097.
[27] E. Tombácz, D. Bica, A. Hajdú, E. Illés, A. Majzik, L. Vékás, Surfactant double layer stabilized magnetic nanofluids for biomedical application, J. Phys.: Condens. Matter 20 (2008) 204103.
[28] W. Jiang, Y. Wu, B. He, X. Zeng, K. Lai, Z. Gu, Effect of sodium oleate as a buffer on the synthesis of superparamagnetic magnetite colloids, J. Colloid Interface Sci. 347 (2010) 1–7.
[29] B. Bateer, Y. Qu, X. Meng, C. Tian, S. Du, R. Wang, K. Pan, H. Fu, Preparation and magnetic performance of the magnetic fluid stabilized by bi-surfactant, J. Magn. Magn. Mater. 332 (2013) 151–156.
[30] J. Sun, S. Zhou, P. Hou, Y. Yang, J. Weng, X. Li, M. Li, Synthesis and characterization of biocompatible $Fe_3O_4$ nanoparticles, J. Biomed. Mater. Res. A 80A (2007) 333–341.
[31] T.K. Jain, M.K. Reddy, M.A. Morales, D.L. Leslie-Pelecky, V. Labhasetwar, Biodistribution, clearance, and biocompatibility of iron oxide magnetic nanoparticles in rats, Mol. Pharm. 5 (2008) 316–327.
[32] R. Massart, Preparation of aqueous magnetic liquids in alkaline and acidic media, IEEE Trans. Magn. 17 (1981) 1247–1248.

[33] A.S. Zahr, M.V. Pishko, Nanotechnology for cancer chemotherapy, in: M.M. Villiers, P. Aramwit, G.S. Kwon (Eds.), Nanotechnology in Drug Delivery, Springer, New York, 2009, pp. 491–518.
[34] A. Hajdú, E. Tombácz, E. Illés, D. Bica, L. Vékás, Magnetite nanoparticles stabilized under physiological conditions for biomedical application, in: Z. Hórvolgyi, E. Kiss (Eds.), Colloids for Nano- and Biotechnology, Springer, Berlin, Heidelberg, 2008, pp. 29–37.
[35] M.A. Morales, A.J.S. Mascarenhas, A.M.S. Gomes, C.A.P. Leite, H.M.C. Andrade, C.M.C. de Castilho, F. Galembeck, Synthesis and characterization of magnetic mesoporous particles, J. Colloid Interface Sci. 342 (2010) 269–277.
[36] T. Belin, N. Guigue-Millot, T. Caillot, D. Aymes, J.C. Niepce, Influence of grain size, oxygen stoichiometry, and synthesis conditions on the $\gamma$–$Fe_2O_3$ vacancies ordering and lattice parameters, J. Solid State Chem. 163 (2002) 459–465.
[37] G. Gnanaprakash, S. Mahadevan, T. Jayakumar, P. Kalyanasundaram, J. Philip, B. Raj, Effect of initial pH and temperature of iron salt solutions on formation of magnetite nanoparticles, Mater. Chem. Phys. 103 (2007) 168–175.
[38] J. Lee, T. Isobe, M. Senna, Preparation of ultrafine $Fe_3O_4$ particles by precipitation in the presence of PVA at high pH, J. Colloid Interface Sci. 177 (1996) 490–494.
[39] B. Veriansyah, J.-D. Kim, B.K. Min, J. Kim, Continuous synthesis of magnetite nanoparticles in supercritical methanol, Mater. Lett. 64 (2010) 2197–2200.
[40] S. Yu, G.M. Chow, Carboxyl group (–$CO_2H$) functionalized ferrimagnetic iron oxide nanoparticles for potential bio-applications, J. Mater. Chem. 14 (2004) 2781–2786.
[41] J.M.D. Coey, Magnetism and Magnetic Materials, Cambridge University Press, New York, 2010.
[42] J.F. de Carvalho, S.N. de Medeiros, M.A. Morales, A.L. Dantas, A.S. Carriço, Synthesis of magnetite nanoparticles by high energy ball milling, Appl. Surf. Sci. 275 (2013) 84–87.
[43] S. Yang, H. Liu, A novel approach to hollow superparamagnetic magnetite/polystyrene nanocomposite microspheres via interfacial polymerization, J. Mater. Chem. 16 (2006) 4480–4487.
[44] C.Y. Wang, J.M. Hong, G. Chen, Y. Zhang, N. Gu, Facile method to synthesize oleic acid-capped magnetite nanoparticles, Chin. Chem. Lett. 21 (2010) 179–182.
[45] L. Zhang, R. He, H.-C. Gu, Oleic acid coating on the monodisperse magnetite nanoparticles, Appl. Surf. Sci. 253 (2006) 2611–2617.
[46] P. Roonasi, A. Holmgren, A Fourier transform infrared (FTIR) and thermogravimetric analysis (TGA) study of oleate adsorbed on magnetite nanoparticle surface, Appl. Surf. Sci. 255 (2009) 5891–5895.
[47] M. Klokkenburg, J. Hilhorst, B.H. Erné, Surface analysis of magnetite nanoparticles in cyclohexane solutions of oleic acid and oleylamine, Vib. Spectrosc. 43 (2007) 243–248.
[48] Y. Sahoo, H. Pizem, T. Fried, D. Golodnitsky, L. Burstein, C.N. Sukenik, G. Markovich, Alkyl phosphonate/phosphate coating on magnetite nanoparticles: a comparison with fatty acids, Langmuir 17 (2001) 7907–7911.
[49] M. Ma, Y. Wu, J. Zhou, Y. Sun, Y. Zhang, N. Gu, Size dependence of specific power absorption of $Fe_3O_4$ particles in AC magnetic field, J. Magn. Magn. Mater. 268 (2004) 33–39.
[50] M.M. Rashad, H.M. El-Sayed, M. Rasly, M.I. Nasr, Induction heating studies of magnetite nanospheres synthesized at room temperature for magnetic hyperthermia, J. Magn. Magn. Mater. 324 (2012) 4019–4023.
[51] C.L. Dennis, A.J. Jackson, J.A. Borchers, R. Ivkov, A.R. Foreman, P.J. Hoopes, R. Strawbridge, Z. Pierce, E. Goerntiz, J.W. Lau, C. Gruettner, The influence of magnetic and physiological behaviour on the effectiveness of iron oxide nanoparticles for hyperthermia, J. Phys. D: Appl. Phys. 41 (2008) 134020.
[52] C.L. Dennis, A.J. Jackson, J.A. Borchers, R. Ivkov, A.R. Foreman, J.W. Lau, E. Goernitz, C. Gruettner, The influence of collective behavior on the magnetic and heating properties of iron oxide nanoparticles, J. Appl. Phys. 103 (2008) 07A319.
[53] C.L. Dennis, A.J. Jackson, J.A. Borchers, P.J. Hoopes, R. Strawbridge, A.R. Foreman, J. van Lierop, C. Grüttner, R. Ivkov, Nearly complete regression of tumors via collective behavior of magnetic nanoparticles in hyperthermia, Nanotechnology 20 (2009) 395103.
[54] L. Lartigue, P. Hugounenq, D. Alloyeau, S.P. Clarke, M. Lévy, J.-C. Bacri, R. Bazzi, D.F. Brougham, C. Wilhelm, F. Gazeau, Cooperative organization in iron oxide multi-core nanoparticles potentiates their efficiency as heating mediators and MRI contrast agents, ACS Nano 6 (2012) 10935–10949.
[55] S. Dutz, M. Kettering, I. Hilger, R. Müller, M. Zeisberger, Magnetic multicore nanoparticles for hyperthermia influence of particle immobilization in tumour tissue on magnetic properties, Nanotechnology 22 (2011) 265102.